35th Annual International Conference of the IEEE EMBS
Osaka, Japan, 3 - 7 July, 2013

# Electric Field Characteristics of Electroconvulsive Therapy with Individualized Current Amplitude: A Preclinical Study

Won Hee Lee, *Student Member, IEEE*, Sarah H. Lisanby, Andrew F. Laine, *Fellow, IEEE*, and Angel V. Peterchev, *Member, IEEE*

*Abstract*—**This study examines the characteristics of the electric field induced in the brain by electroconvulsive therapy (ECT) with individualized current amplitude. The electric field induced by bilateral (BL), bifrontal (BF), right unilateral (RUL), and frontomedial (FM) ECT electrode configurations was computed in anatomically realistic finite element models of four nonhuman primates (NHPs). We generated maps of the electric field strength relative to an empirical neural activation threshold, and determined the stimulation strength and focality at fixed current amplitude and at individualized current amplitudes corresponding to seizure threshold (ST) measured in the anesthetized NHPs. The results show less variation in brain volume stimulated above threshold with individualized current amplitudes (16–36%) compared to fixed current amplitude (30–62%). Further, the stimulated brain volume at amplitude-titrated ST is substantially lower than that for ECT with conventional fixed current amplitudes. Thus individualizing the ECT stimulus current could compensate for individual anatomical variability and result in more focal and uniform electric field exposure across different subjects compared to the standard clinical practice of using high, fixed current for all patients.**

## I. Introduction

ELECTROCONVULSIVE therapy (ECT) is the most effective treatment for severe major depression [1]. ECT induces a generalized seizure under anesthesia by delivering electric current to the brain via electrodes placed on the scalp. However, the use of ECT is impeded by cognitive side effects such as amnesia [2] and, less commonly, cardiac complications [3]. Various ECT technique modifications have been proposed to reduce adverse side effects while maintaining therapeutic efficacy. However, there is still limited knowledge of how to optimally determine the dosing of ECT. The ECT dose includes electrode placement/shape and stimulus current parameters (e.g., current amplitude or polarity) which affect the electric field (E-field) induced in the brain. The distribution of the E-field in the brain also depends upon the geometry of the head and the electrical properties of head tissues [4]-[6].

In practice, ECT is applied with fixed high current amplitude (800 or 900 mA). Conventional ECT current amplitudes produce widespread direct stimulation in the brain that exceeds the neural activation threshold by several fold [6]. Furthermore, using fixed current amplitude for all patients may lead to variable clinical outcomes due to individual anatomical and neurophysiological variation [7]. Indeed, there is considerable variability in clinical outcomes (efficacy as well as adverse cognitive side effects), which at present do not have a known anatomical or physiological explanation. Therefore, we propose that lowering and individualizing stimulus current amplitude could serve as a means of reducing side effects and clinical outcome variability [5, 8, 9].

Previously, using a single nonhuman primate (NHP) model, we studied the suprathreshold direct stimulation strength and volume (focality) in ECT with individualized current amplitude [5]. In this paper, we extend our previous single-subject work to investigate the E-field characteristics of various forms of ECT with individualized current amplitude in four NHP subjects. The E-field strength generated by these modalities is computed in anatomically realistic finite element models of the four NHP heads. We determine the stimulation strength and focality relative to an empirical E-field neural activation threshold at fixed stimulus current amplitude and at individualized current amplitudes corresponding to amplitude-titrated seizure threshold (ST). Understanding the induced E-field characteristics and their individual variability could help identify potential causes of the differences in clinical outcome, and could support the development of ECT dosing paradigms with fewer side effects.

## II. Methods

### A. High-resolution ECT Head Model Generation

All studies were approved by the Institutional Animal Care and Use Committees of New York State Psychiatric Institute, Columbia University, and Duke University. Anatomically realistic NHP head models were created from T1-weighted magnetic resonance imaging (MRI) ($0.7\times0.7\times0.7$ mm$^3$ voxel) and diffusion tensor imaging ($1.4\times1.4\times1.4$ mm$^3$ voxel) data sets of the four healthy male rhesus macaques (*Macaca mulatta*) (age=12–18 years; weight=8.4–10.7 kg) acquired on a Siemens 3 T Trio scanner using an 8-channel knee coil. We previously developed a processing pipeline for deriving a realistic finite element model of a NHP head incorporating

This work was supported by NIH grant R01MH091083.

W. H. Lee is with the Department of Biomedical Engineering, Columbia University, New York, NY 10027 and with the Department of Psychiatry and Behavioral Sciences, Duke University, Durham, NC 27710, USA (e-mail: wl2324@columbia.edu).

S. H. Lisanby is with Department of Psychiatry and Behavioral Sciences, and Department of Psychology & Neuroscience, Duke University, Durham, NC 27710, USA (e-mail: sarah.lisanby@duke.edu).

A. F. Laine is with the Department of Biomedical Engineering, Columbia University, New York, NY 10027, USA (e-mail: laine@columbia.edu).

A. V. Peterchev is with Departments of Psychiatry and Behavioral Sciences, Biomedical Engineering, and Electrical and Computer Engineering, Duke University, Durham, NC 27710, USA (phone: 919-684-0383; fax: 919-681-9962; e-mail: angel.peterchev@duke.edu).

978-1-4577-0216-7/13/$26.00 ©2013 European Union

tissue heterogeneity and tissue conductivity anisotropy [5]. The processing framework consists of three main components: preprocessing, tissue segmentation, and finite element mesh generation. The preprocessing of the structural MR images includes AC-PC spatial alignment, bias field correction, anisotropic diffusion filtering, and skull stripping [5, 10]. Individual tissue probability maps corresponding to gray matter, white matter, and cerebrospinal fluid (CSF) were automatically produced using SPM8 [11]. Manual segmentation of the non-brain regions into 11 tissue compartments, representing skin, muscle, skull spongiosa, skull compacta, vertebrae, spinal cord, lens, eyeball, sclera, optic nerve, and sinus, was carried out using a combination of tools from the ITK-SNAP software [12] and an in-house morphological algorithm. Subsequently, the realistically-shaped stimulation electrodes for the BL (3.5 cm diameter) and BF, RUL, and FM (2.5 cm diameter, respectively) ECT configurations were created and placed on the NHP head models (see Fig. 1) [5]. Finally, adaptive finite element meshes were generated for each subject using the restricted Delaunay tessellation algorithm [13], resulting in the four subject-specific finite element models of the rhesus macaque heads and electrodes, each consisting of approximately 1.8 million tetrahedral elements.

### B. Tissue Electrical Conductivity

The isotropic electrical conductivity values listed in Table I [5] were assigned to all tissue compartments except the white matter which was treated as anisotropic. The white matter conductivity tensors $\sigma$ were computed from the measured diffusion tensors $D$ and the isotropic white matter conductivity $\sigma_{iso}$ from the literature using the volume normalized approach [14, 15]: In each voxel, the diffusion tensor is linearly scaled so that the volume of the resulting conductivity tensor ellipsoid matches that of an isotropic conductivity tensor sphere with radius $\sigma_{iso}$

$$\sigma = \frac{\sigma_{iso}}{\sqrt[3]{d_1 \cdot d_2 \cdot d_3}} D \quad (1)$$

where $d_i$ are the diffusion tensor eigenvalues. This approach preserves the orientation (eigenvectors) and anisotropy ratios (eigenvalue ratios) of the diffusion tensors.

### C. Electric Field Solution

Each of the realistic finite element models along with the electrical conductivity values was imported into the finite element analysis software ANSYS (ANSYS Inc., Canonsburg, PA, USA). For all ECT electrode configurations, we acquired the forward E-field solution by solving the quasi-static Laplace equation with no internal sources [16]

$$\nabla \cdot (\sigma \nabla V) = 0 \quad (2)$$

where $V$ and $\sigma$ denote the electric potential and tissue electrical conductivity tensor, respectively. The linear equation system of the finite element method was solved using the preconditioned conjugate gradient solver within ANSYS. The E-field distribution was determined by taking the gradient of the scalar potential $V$.

TABLE I
TISSUE ELECTRICAL CONDUCTIVITIES (S/M)

| Tissue | Conductivity | Tissue | Conductivity |
|---|---|---|---|
| Skin | 0.43 | Lens | 0.32 |
| Muscle | 0.32 | Eyeball | 0.5 |
| Skull compacta | 0.0063 | Sclera | 0.5 |
| Skull spongiosa | 0.04 | Spinal cord | 0.15 |
| Cerebrospinal fluid | 1.79 | Vertebrae | 0.012 |
| Gray matter | 0.33 | Optic nerve | 0.14 |
| White matter (iso.) | 0.14 | Sinus | 0 |

### D. In Vivo Motor and Seizure Threshold Titration

The detailed methodology of titrating MT and ST was presented previously [5, 8]. In summary, MT and ST were titrated by adjusting the current amplitude (pulse width = 0.2 ms) for each ECT electrode configuration in the four NHP subjects. The MT was defined as the minimum stimulus pulse amplitude needed to achieve a 50 μV peak-to-peak motor-evoked potential in the first dorsal interosseous (FDI) muscle for at least five out of ten trials. MT was measured for both current polarities and the two values were averaged. ST was titrated by incrementing the stimulus current amplitude while holding all the other stimulus parameters fixed (50 pulses/s, 10 s train duration). The MT and ST titration was repeated three times for each ECT condition in each subject.

### E. Stimulation Strength and Focality Analysis

An individual neural activation threshold $E_{th}$ was determined from the median E-field strength in the FDI areas of motor cortex at current amplitude corresponding to individual MT for the RUL electrode configuration [5, 17]. We computed maps of stimulation strength relative to threshold by dividing the E-field magnitude distribution in the brain by the threshold, $E/E_{th}$ [5, 6].

We quantified the focality of stimulation by the percentage of the brain volume that is exposed to E-field strong enough to produce suprathreshold depolarization, i.e., the volume where $E/E_{th} \geq 1$ [6]. For each ECT electrode configuration we explored the variation in the stimulated brain volume above the E-field threshold across the four subjects for individualized ST current amplitudes as well as for fixed current amplitude corresponding to the average ST.

## III. RESULTS

Table II gives the measured RUL MTs and the amplitude-titrated STs for the four ECT electrode configurations. All values are the averages of three measurements. The individual neural activation threshold was estimated to be $E_{th}$ = 0.35, 0.52, 0.44, and 0.48 V/cm for subject MA, CH, DY, and RZ, respectively [17].

Fig. 1 shows the simulated BL, BF, RUL, and FM ECT electrode placements in one subject (CH; left column), and coronal cross-sectional plots of the E-field magnitude distributions relative to the neural activation threshold $E_{th}$ at current strengths corresponding to individually-titrated ST for the four subjects (second to fifth columns, respectively).

Fig. 2 (a) shows the percentage of brain volume stimulated above threshold at individual ST. The results indicate that BL

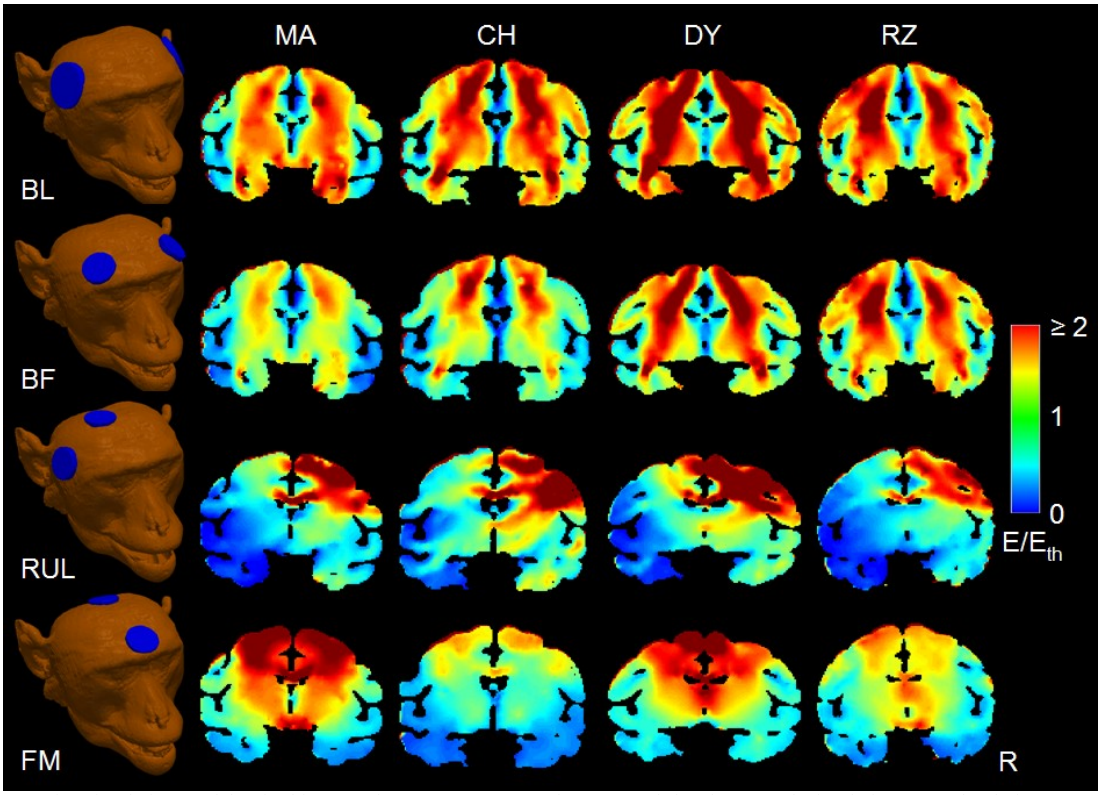


Fig. 1. Representative simulation models of subject CH for BL, BF, RUL, and FM ECT (left column) and stimulation strength relative to neural activation threshold ($E_{th}$) at current amplitude corresponding to seizure threshold for BL, BF, RUL and FM electrode configurations (top to bottom rows, respectively) in each subject (second to fifth columns, respectively). R: right.

ECT stimulates the largest brain volume (53–77%) in all subjects. On the other hand, RUL produces the most focal stimulation (19–33%) in all subjects except subject CH whose lowest stimulated brain volume is for FM ECT. Fig. 2 (b) compares the coefficient of variation of the stimulated brain volume across subjects for ECT with individualized and fixed (average ST across subjects) current amplitude, indicating that for all electrode configurations, individualized current amplitude results in less variability of the stimulated brain volume across subjects.

TABLE II
AVERAGE MOTOR THRESHOLD (MA) AND AVERAGE SEIZURE THRESHOLD (MA) FOR FOUR ECT CONFIGURATIONS IN FOUR NHP SUBJECTS

| Subject | Motor Threshold (mA) | Seizure Threshold (mA) | | | |
|---|---|---|---|---|---|
| | RUL | BL | BF | RUL | FM |
| MA | 50 | 111 | 92 | 114 | 89 |
| CH | 120 | 215 | 190 | 284 | 145 |
| DY | 82 | 222 | 196 | 190 | 136 |
| RZ | 70 | 164 | 155 | 141 | 95 |
| Mean | 81 | 178 | 158 | 182 | 116 |

## IV. DISCUSSION AND CONCLUSIONS

We investigated the E-field characteristics of various ECT electrode configurations with fixed and individualized current amplitudes using four high-resolution anatomically accurate finite element NHP head models. The results in Fig. 1 illustrate the different stimulation patterns in the brain resulting from the various ECT electrode configurations at the lowest current strength required to induce a seizure (ST). Different E-field patterns suggest different loci of seizure induction which may be important for focal brain stimulation.

Fig. 2 (a) shows that the largest portion of the brain in all subjects is stimulated by BL ECT even at the lowest current strength that induces a seizure (ST). In contrast, the RUL ECT electrode configuration with individualized current results, on average, in the most focal stimulation and E-field distribution shifted to the right hemisphere, thereby potentially sparing left hemisphere regions from adverse side effects of stimulation. These observations are consistent with our previous findings [5].

Notably, the brain volumes stimulated at amplitude-titrated ST are substantially smaller than the volumes stimulated with conventional fixed current strengths that may reach 100% [4, 16]. Thus, seizures can be generated with lower currents, corresponding to more focal stimulation than those in standard ECT.

Fig. 2 (b) indicates that ECT with individualized current strength results in variation in the brain volume stimulated above neural activation threshold across subjects that is ~1.7–2.1 times smaller than the variation for fixed current strength. This suggests that current amplitude individualization could be a means of compensating for interindividual variability in anatomy and neurophysiological excitability. This observation supports exploring individualization of the ECT stimulus current amplitude in clinical studies. Therefore, ECT with low, individualized current should be explored as a means of reducing side effects and outcome variability in clinical studies.

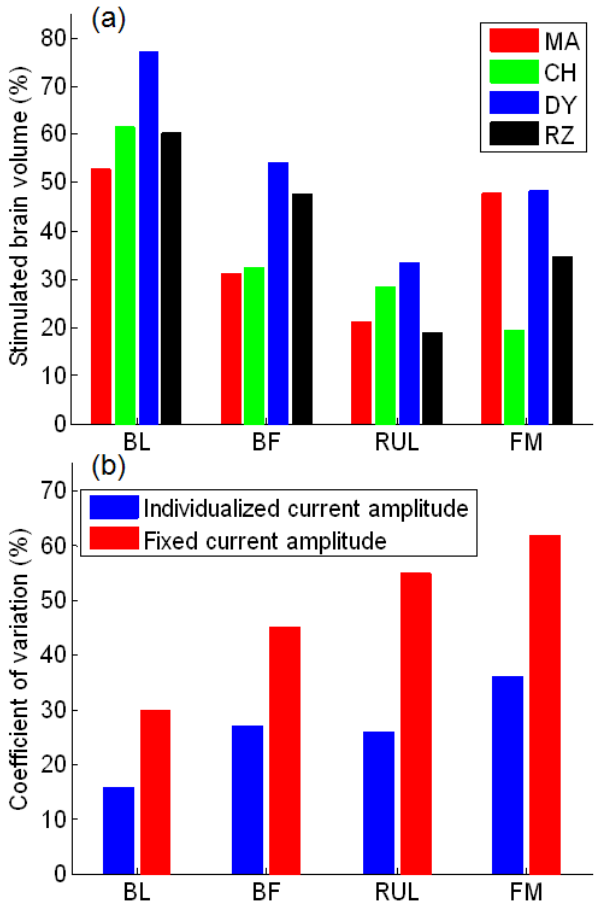


Fig. 2. (a) Percentage brain volume stimulated above threshold ($E \geq E_{th}$) at individual ST for four subjects and four electrode configurations and (b) coefficient of variation of the stimulated brain volume across subjects for individualized and fixed (average ST) current amplitude for the four ECT electrode configurations.

## V. Acknowledgement

The authors thank Christopher Sikes-Keilp, Mohamed Aly, Brian Chan, Niko Reyes, Moacyr A. Rosa, and Nagy Youssef for assisting in the NHP procedures and data entry. We would like to thank Drs. Richard Weiner and Andrew Krystal from the Department of Psychiatry and Behavioral Sciences at Duke University for their helpful comments and suggestions.

## VI. References

[1] R. Abrams, *Electroconvulsive therapy*, 4th Ed. New York: Oxford Unversity Press, 2002.

[2] H. A. Sackeim, J. Prudic, R. Fuller, J. Keilp, P. W. Lavori, and M. Olfson, "The cognitive effects of electroconvulsive therapy in community settings," *Neuropsychopharmacology,* vol. 32, pp. 244-254, 2007.

[3] G. A. Nuttall, M. R. Bowersox, S. B. Douglass, J. McDonald, L. J. Rasmussen, P. A. Decker, W. C. Oliver, and K. G. Rasmussen, "Morbidity and mortality in the use of electroconvulsive therapy," *J. ECT,* vol. 20, pp. 237-241, 2004

[4] Z. D. Deng, S. H. Lisanby, and A. V. Peterchev, "Effect of anatomical variability on neural stimulation strength and focality in electroconvulsive therapy (ECT) and magnetic seizure therapy (MST)," *Conf. Proc. IEEE Eng. Med. Biol. Soc.,* vol. 2009, pp. 682-688, 2009.

[5] W. H. Lee, S. H. Lisanby, A. F. Laine, and A. V. Peterchev, "Stimulaton strength and focality of electroconvulsive therapy with individualized current amplitude: a preclinical study," *Conf. Proc. IEEE Eng. Med. Biol. Soc., pp. 6430-6433, 2012.*

[6] Z. D. Deng, S. H. Lisanby, and A. V. Peterchev, "Electric field strength and focality in electroconvulsive therapy and magnetic seizure therapy: a finite element simulation study," *J. Neural Eng.,* vol. 8, 2011.

[7] A. V. Peterchev, M. A. Rosa, Z. D. Deng, J. Prudic, and S. H. Lisanby, "Electroconvulsive therapy stimulus parameters: rethinking dosage," *J. ECT,* vol. 26, pp. 159-174, 2010.

[8] A. V. Peterchev, B. Chan, and S. H. Lisanby, "Pulse amplitude adjustment: a novel means of individualizing and predicting dosage requirements for electroconvulsive therapy and magnetic seizure therapy," *J. ECT,* vol. 26, p. 154, 2010.

[9] M. A. Rosa, G. L. Abdo, S. H. Lisanby, and A. V. Peterchev, "Seizure induction with low-amplitude-current (0.5A) electroconvulsive therapy," *J. ECT,* vol. 27, pp. 341-342, 2011.

[10] W. H. Lee, T. S. Kim, M. H. Cho, Y. B. Ahn, and S. Y. Lee, "Methods and evaluations of MRI content-adaptive finite element mesh generation for bioelectromagnetic problems," *Phys. Med. Biol.,* vol. 51, pp. 6173-6186, 2006.

[11] J. Ashburner and K. J. Friston, "Unified segmentation," *NeuroImage,* vol. 26, pp. 839-851, 2005.

[12] P. A. Yushkevich, J. Piven, H. C. Hazlett, R. G. Smith, S. Ho, J. C. Gee, and G. Gerig, "User-guided 3D active contour segmentation of anatomical structures: significantly improved efficiency and reliability," *NeuroImage,* vol. 31, pp. 1116-1128, 2006.

[13] J. P. Pons, E. Segonne, J. D. Boissonnat, L. Rineau, M. Yvinec, and R. Keriven, "High-quality consistent meshing of multi-label datasets," *Inf. Process. Med. Imaging,* vol. 20, pp. 198-210, 2007.

[14] D. S. Tuch, V. J. Wedeen, A. M. Dale, J. S. George, and J. W. Belliveau, "Conductivity tensor mapping of the human brain using diffusion tensor MRI," *Proc. Natl. Acad. Sci.,* vol. 98, pp. 11697-11701, 2001.

[15] H. Hallez, S. Staelens, and I. Lemahieu, "Dipole estimation errors due to not incorporating anisotropic conductivities in realistic head models for EEG source analysis," *Phys. Med. Biol.,* vol. 54, pp. 6079-6093, 2009.

[16] W. H. Lee, Z. D. Deng, T. S. Kim, A. F. Laine, S. H. Lisanby, and A. V. Peterchev, "Regional electric field induced by electroconvulsive therapy in a realistic finite element head model: influence of white matter anisotropic conductivity," *NeuroImage,* vol. 59, pp. 2110-2123, 2012.

[17] W. H. Lee, S. H. Lisanby, A. F. Laine, and A. V. Peterchev, "Anatomical variability predicts individual differences in transcranial electric stimulation motor threshold," *Conf. Proc. IEEE Eng. Med. Biol. Soc., Conf. Proc. IEEE Eng. Med. Biol. Soc., 2013.*